MODELLING AND EXPERIMENTAL TESTS OF A COPPER THERMOSYPHON

ABSTRACT. Electrical energy, solar energy, and/or direct combustion of a fuel are the main thermal sources for home water heating. In recent years, the use of solar energy has become popular because it is a renewable and economic energy. Among the solar collectors, the collectors assisted by thermosyphons are more efficient; therefore, they can enhance the heat transfer to water. A thermosyphon is basically a sealed tube filled with a working fluid and normally have three regions: the evaporator, the adiabatic section and the condenser. The great advantage of this device is that the thermal resistance to heat transfer between its regions is very small, and as a result, there is a small temperature difference. This article aims to model a thermosyphon using correlations based on its operation limits. This modelling will be used as a design tool for compact solar collectors assisted by thermosyphons. Based on the results obtained with the mathematical modelling, one copper thermosyphon, with deionized water as the working fluid, was developed and experimentally tested. The tests were carried out for a heat load varying from 30 to 60W in a vertical position. The theoretical and experimental results were compared to verify the mathematical model.

KEYWORDS: solar collector, thermosyphons, operation limit, experiment.

MODELAGEM E TESTES EXPERIMENTAIS DE UM TERMOSSIFÃO DE COBRE

RESUMO. Energia elétrica, energia solar e/ou combustão direta de um combustível são as principais fontes térmicas para aquecimento doméstico de água. Nos últimos anos, a utilização de energia solar tornou-se popular porque ela é uma energia renovável e econômica. Dentre os coletores solares, os coletores assistidos por termossifões são os mais eficientes, portanto, eles podem melhorar a transferência de calor para a água. Um termossifão é basicamente um tubo selado preenchido com um fluido de trabalho e, normalmente, possui três regiões: o evaporador, a seção adiabática e o condensador. A grande vantagem deste dispositivo é que a resistência térmica para a transferência de calor entre suas regiões é muito pequena e, como resultado, existe uma pequena diferença de temperatura. Este artigo tem como objetivo modelar um termossifão utilizando correlações baseadas em seus limites de operação. Esta modelagem será utilizada como uma ferramenta de projeto para coletores solares compactos assistidos por termossifões. Baseado nos resultados obtidos com o modelo matemático, um termossifão de cobre, com água deionizada como fluido de trabalho, foi desenvolvido e testado experimentalmente. Os testes foram realizados para uma potência variando de 30 a 60 W em uma posição vertical. Os resultados teóricos e experimentais foram comparados para verificar o modelo matemático.

PALAVRAS-CHAVE: coletor solar, termossifões, limite de operação, investigação experimental.

INTRODUCTION

Water heating systems for domestic use in Brazil can have an energy source of electrical energy, solar energy and/or direct burning of a particular fuel (LPG or natural gas) in a gas burner. Due to the water crisis that the country is facing, the high cost of heating water by electricity is increasingly being replaced by heating through fuel combustion in a gas burner or by the use of a solar collector; and in some cases, both technologies are used together.

The most common solar collector used in Brazil is the flat plate. This type of solar collector has Brazilian technology, however they occupy too much area on building roof tops. A more thermally efficient solar collector is the evacuated tube solar collector (thermosyphon solar collector). This type of solar collector is more efficient because they use thermosyphons in order to enhance the transfer of heat for water heating. However, there are few applications of thermosyphon solar collectors in Brazil and the Brazilian companies do not have the manufacturing technology.

Several researchers have studied the application of heat pipes and thermosyphons in solar collectors for heating water in the interest of domestic use with different configurations (Oliveti & Arcuri, 1996; Ismail & Abogderah, 1998; Hussein, Mohamad & El-Asfouri, 1999a, 1999b).

The solar collectors tested by Oliveti and Arcuri (1996) and by Hussein et al. (1999a, 1999b) were assisted by thermosyphons with water as the working fluid. On the other hand, Ismail and Abogderah (1998) used heat pipes with methanol as the working fluid in the solar collectors. Abreu and Colle (2004) presented a different configuration of the settings above. While the other researchers used straight tube thermosyphons, Abreu and Colle (2004) developed a condenser with curved geometry to allow a better coupling between the condenser region and the heat sink.

Azad (2008) accomplished a theoretical and experimental study on the thermal performance of thermosyphon solar collectors. He worked on a copper collector with six thermosyphons with an external diameter of 12.7 mm and a length of 1,850 mm. The tests were performed outdoor in Tehran (Iraq) and the thermal efficiency was based on ASHRAE 93-1986 method.

Chien et al. (2010) also made a theoretical and experimental study regarding a solar collector assisted by thermosyphons. They used the method of equivalent thermal resistances for the theoretical study, and for the experiment, they tested the solar collectors under different inclination angles and heat loads.

Azad (2012) manufactured three heat pipe solar collectors with tubes of different shapes and with a total length ranging from 1.55 to 1.90 m. All heat pipes used a stainless steel wire mesh of 100 and ethanol as the working fluid. The solar collectors were tested outdoor in Tehran (Iraq).

Du, Hu and Kolhe (2013) manufactured a solar collector assisted by twenty heat pipes and tested it outdoor in Nanjing (China). Each heat pipe had an evaporator outer diameter of 8 mm and length of 1,660 mm, and a condenser outer diameter of 14 mm and length of 83 mm. The heat pipes were inserted into a borosilicate glass tube with a diameter of 70 mm and a length of 1,730 mm. In the annular space between the glass tube and an evacuation process was accomplished up to 0.05 Pa (absolute pressure).

Deng et al. (2013) constructed and tested a solar collector assisted by an array of micro heat pipes made of aluminum. The heat pipes used acetone as the working fluid and the capillary structure was composed by grooves with hydraulic diameter varying between 0.4 and 1.0 mm.

According to this review, the development process of thermosyphons and heat pipes for solar collectors is not presented. In other words, for this specific application, the manufacturing process as well as the necessary experimental tests for qualifying these kinds of devices are not shown. Thus, this paper aims to present the steps to develop thermosyphons for application in solar collectors.

OPERATION LIMIT MODEL FOR THERMOSYPHONS

The mathematical model presented here consists of determining the operational limits for thermosyphons. These limits are entrainment, sonic, viscous, drying, and boiling. For each one of them, specific correlations will be used for their evaluations.

One thermosyphon is schematically represented in Figure 1, which is composed by three regions: the evaporator section (where the heat load is supplied), the adiabatic section, and the condenser section (where the heat is removed). The thermosyphon works in the following way: first, heat is supplied in the evaporator section causing the vaporization of the inner working fluid; second, due to the pressure difference, the generated vapor flows to the thermosyphon cooled region (condenser section) where heat is rejected to the cold source (water or air flow passing outside the tubes) and the vapor condenses inside; third, the condensate fluid returns to the evaporator by gravity, completing the cycle.

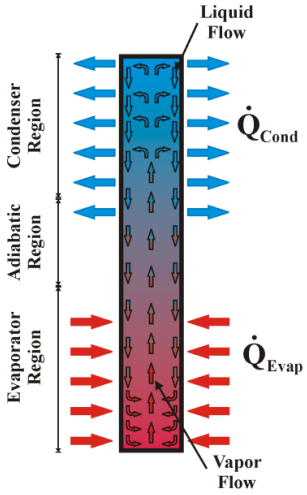

Figure 1. Schematic representation of a typical thermosyphon.

Since the thermosyphon is assisted by gravity, the condenser region must be located above the evaporator region at a minimal tilt angle. The adiabatic region is located between the evaporator and the condenser (it has variable size or may not exist in some cases).

Operation Limit Model

The limit model was implemented and simulated using the software EES™ (Engineering Equation Solver™).

Entrainment limit

As the heat load applied to the evaporator is increased, the vapor velocity increases and may reach a higher velocity than the liquid velocity. That is, the shear forces on the liquid-vapor interface can be significant. Thus, if the shear forces are greater than the forces caused by the liquid surface tension, droplets can be dragged from the liquid. As a consequence, the entrainment limit can be reached.

The entrainment limit estimates the maximum value of heat transfer rate that this effect begins to take place within the thermosyphon. The main causes for this limit to be reached is the excess of working fluid in the condenser or the lack of working fluid in the evaporator.

According to Groll and Rösler (1992) and Mantelli (2013), some expressions have been developed for the entrainment limit estimation. The correlation shown in Eq. (1) has been proposed for determining the maximum heat transfer for the entrainment limit.

$$\dot{Q}_{max,entrainment} = f_1\, f_2\, f_3\, h_{lv} A_v\, \rho_v^{1/2} \left[\left(\rho_l - \rho_v \right) g\, \sigma \right]^{1/4}, \qquad (1)$$

where, f_1, f_2, and f_3 are parameters listed as follow; h_{lv} is the vaporization latent heat; ρ_v is the vapor mass density; ρ_l is the liquid mass density; g is the gravitational acceleration; σ is the surface tension; and A_v is the vapor core area.

The parameter f_1 is the Bond number (*Bo*), Eq. (2), defined as the ratio between gravity and tension forces,

$$Bo = d_i \left[\frac{(\rho_l - \rho_v) g}{\sigma} \right]^{1/2}, \tag{2}$$

where, d_i is the tube inner diameter.

The parameter f_2 is a function of the dimensionless parameter K_p, given by Eq. (3):

$$K_p = \frac{p_v}{\left[(\rho_l - \rho_v) g \sigma \right]^{1/2}}, \tag{3}$$

where, p_v is the vapor pressure.

For $K_p \leq 4.10^4$, $f_2 = K_p{}^{-0.17}$ and for $K_p > 4.10^4$, $f_2 = 0.165$.

The parameter f_3 is a factor which corrects the Eq. (1) for the thermosyphon inclination and it is also a function of the Bond number. According to Mantelli (2013) for vertical position, $f_3 = 1$.

Sonic limit

The sonic limit represents the heat applied to the thermosyphon when vapor reaches sonic velocity. It can be more commonly achieved by thermosyphons using liquid metal as the working fluid and it is influenced by the size of the vapor core. Sonic limits can be reached during the start-up and at steady state conditions. If this limit is reached, the vapor usually located in the core of the thermosyphon is blocked by a shock wave. This phenomenon causes a temperature increase in this region and can be expressed by Eq. (4) which was proposed by Busse (1973):

$$\dot{Q}_{max,sonic} = 0.474 h_{lv} A_v \left(\rho_v p_v \right)^{1/2}. \tag{4}$$

Viscous limit

In situations in which the thermosyphon works at low temperature levels, the pressure gradient between the evaporator and the condenser is very small. When the forces caused by such low pressure gradient are lower than the viscous forces, vapor flow does not take place in the thermosyphon. That characterizes the viscous limit. Busse (1973) proposed a correlation, Eq. (5), for this limit:

$$\dot{Q}_{max,viscous} = d_v^2\, h_{lv} A_v \left(\frac{\rho_v p_v}{64\, \mu_v l_{eff}} \right), \tag{5}$$

where, d_v is the vapor core diameter, μ_v is the vapor dynamic viscosity, and l_{eff} is the effective length given by

$$l_{eff} = l_a + 0.5\left(l_e + l_c\right). \tag{6}$$

where, l_a is the adiabatic section length, l_e is the evaporator region length, and l_c is the condenser region length.

Boiling limit

The boiling limit occurs when there is a large amount of working fluid in the thermosyphon and the evaporator region is heated with high heat fluxes. It occurs at the transition between the boiling processes of pool boiling and evaporation in film when the heat flux is critical. As a result, bubbles are formed and adhered to this film, causing insulation of the inner pipe wall. Since the vapor thermal conductivity is low, the wall temperature increases and it may reach, at extreme cases, the melting point of the metal material. An expression is proposed in Peterson (1994), Eq. (7), to estimate the maximum heat transfer rate for the boiling limit:

$$\dot{Q}_{max,boiling} = 0.12\, h_{lv} A_e \left[\rho_v^2 \left(\rho_l - \rho_v\right) g\, \sigma \right]^{1/4} . \tag{7}$$

where, A_e is the evaporator area.

HEAT TRANSFER ANALYSIS

This section presents the heat transfer analysis based on the correlations using the experimental data as input.

Calculation of the heat transferred to the thermosyphon

In order to calculate the heat transfer rate that is transferred to the thermosyphon, a control volume is established according to Figure 2.

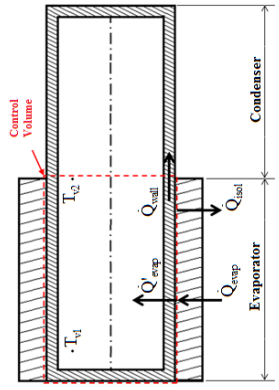

Figure 2. Energy balance in evaporator section.

Applying an energy balance in the control volume of Figure 2, the Eq. (8) can be obtained:

$$\dot{Q}'_{evap} = \dot{Q}_{evap} - \dot{Q}_{isol} - \dot{Q}_{wall}\,, \tag{8}$$

where, $\dot{Q}_{evap}$ is the heat transfer rate supplied to the evaporator by the heat system (skin heater/electric resistor), Eq. (9); $\dot{Q}_{wall}$ is the heat transfer rate lost axially through the tube wall, Eq. (10); and $\dot{Q}_{isol}$ is the heat transfer rate lost through the insulation, Eq. (11).

$$\dot{Q}_{evap} = IV\,, \tag{9}$$

$$\dot{Q}_{isol} = k_{Cu} A_w \left(\frac{\bar{T}_{eo} - \bar{T}_{co}}{l_{eff}} \right), \tag{10}$$

$$\dot{Q}_{wall} = A_{isol}\, \bar{h}_{isol,o} \left(\bar{T}_{isol,o} - \bar{T}_{env} \right), \tag{11}$$

where, I is the electric current, V is the voltage, k_{Cu} is the copper thermal conductivity, A_w is the wall cross area, $\bar{T}_{eo}$ is the outer evaporator average temperature, $\bar{T}_{co}$ is the outer condenser average temperature, A_{isol} is the insulation area, $\bar{h}_{isol,o}$ is the outer insulation average heat transfer coefficient, $\bar{T}_{isol,o}$ is the outer insulation average temperature, and $\bar{T}_{env}$ is the environment average temperature.

According to Bergman, Lavine, Incropera and DeWitt (2012) the heat transfer coefficient by natural convection at outer insulation can be estimated by the Eqs. (12) and (13), Churchill and Chu's correlation. That is,

$$\overline{Nu}_D = \frac{\bar{h}_{isol,o}\, d_{isol,o}}{k_{air}}\,, \tag{12}$$

$$\overline{Nu}_D = \left\{ 0.60 + \frac{0.387\, Ra_D^{1/6}}{\left[1 + \left(\frac{0.559}{Pr} \right)^{9/16} \right]^{9/27}} \right\}^2, \tag{13}$$

where, $\overline{Nu}_D$ is the average Nusselt number, $d_{isol,o}$ is the outer insulation diameter, k_{air} is the air thermal conductivity, Ra_D is the Rayleigh number, and Pr is the Prandtl number.

Mass transfer rate of the internal flow

The calculation of the thermosyphon's internal mass transfer rate, $\dot{m}_i$, can be estimated by Eq. (14), neglecting the sensible heat variation along the evaporator region [$\dot{m}_i h_{lv} \gg \dot{m}_i c_{p,l} \left(T_{v2} - T_{v1} \right)$].

$$\dot{m}_i = \frac{\dot{Q}'_{evap}}{h_{lv}}. \tag{14}$$

Heat transfer coefficient calculation for the internal region of the condenser

To determine the internal heat transfer coefficient for the condenser region, the operation temperature must be primarily estimated. Thus, an equivalent thermal circuit presented in Figure 3 is proposed for determining the operation temperature T_{op}.

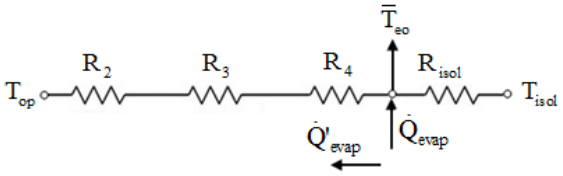

Figure 3. Equivalent thermal circuit

where, R_2 is the thermal resistance associated to the wall conduction, Eq. (15); R_3 is the thermal resistance associated to the inner evaporation, Eq. (16), for pool boiling Eq. (17) and for evaporation in film, Eq. (18); and R_4 is the thermal resistance associated to the liquid-vapor interface, Eq. (19),

$$R_2 = \frac{ln\left(\frac{d_o}{d_i}\right)}{2\pi l_e k_{Cu}}; \tag{15}$$

$$R_3 = R_{3p}F + R_{3f}\left(1-F\right); \tag{16}$$

$$R_{3p} = \frac{1}{g^{0.2}\phi\dot{Q}^{0.4}\left(\pi d_i l_e\right)^{0.6}}, \tag{17}$$

$$R_{3f} = \frac{0.345\dot{Q}^{1/3}}{d_i^{4/3}g^{1/3}l_e\Psi^{4/3}}. \tag{18}$$

$$R_4 = \frac{RT_{op}{}^2\left(2\pi RT_{op}\right)^{1/2}}{h_{lv}^2 p_v A_e}; \tag{19}$$

where, d_o is outer diameter, F is filling ratio (defined as the ratio between the volume of working fluid and volume of the evaporator), R is the universal gas constant, T_{op} is the operating temperature, ϕ and Ψ are given by

$$\phi = \frac{\rho_l^{0.65}k_l^{0.3}c_{p,l}^{0.7}}{\rho_v^{0.25}h_{lv}^{0.4}\mu_l^{0.1}}\left(\frac{p_v}{p_{atm}}\right)^{0.23}; \tag{20}$$

$$\Psi = \left(\frac{h_{lv} k_l^3 \rho_l^2}{\mu_l} \right)^{1/4}; \quad (21)$$

where, k_l is the liquid thermal conductivity, $c_{p,l}$ is the liquid specific heat at constant pressure, and μ_l is the liquid dynamic viscosity.

Therefore, based on the analysis of the equivalent thermal circuit, the Eq. (22) can be determined as:

$$T_{op} = \bar{T}_{eo} - \dot{Q}'_{evap} \left(R_2 + R_3 + R_4 \right). \quad (22)$$

In order to estimate the internal heat transfer coefficient into the condenser area, the condensate thermal resistance, R_{cond}, can be used. This thermal resistance is given by Eq. (23).

$$R_{cond} = \frac{0.345 \dot{Q}'^{1/3}_{evap}}{d_i^{4/3} g^{1/3} l_c \Psi^{4/3}}, \quad (23)$$

However, R_{cond}, can also be estimated using Eq. (24):

$$R_{cond} = \frac{1}{\left(\bar{h}_{i,1}^{cond} A_i^{cond} \right)} \quad (24)$$

where $\bar{h}_{i,1}^{cond}$ is condenser internal average heat transfer coefficient at point #1 and A_i^{cond} is the condenser inner area.

Mantelli (2013) state that the inner average heat transfer coefficient in the condenser can be estimated by Eqs. (25) to (27):

$$\overline{Nu}_i^{cond} = \frac{\bar{h}_{i,2}^{cond} d_i}{k_l}, \quad (25)$$

$$\overline{Nu}_i^{cond} = 25 \left(Re_i^{cond} \right)^{0.25} Pr_l^{0.4}, \quad (26)$$

$$Re_i^{cond} = \frac{4 \dot{Q}'_{evap}}{\pi d_i h_{lv} \mu_l}, \quad (27)$$

where, $\overline{Nu}_i^{cond}$ is the condenser inner average Nusselt number, $\bar{h}_{i,2}^{cond}$ is condenser inner average heat transfer coefficient at point #2, Re_i^{cond} is the condenser inner Reynolds number and Pr_l is the liquid Prandtl number.

EXPERIMENT

The methodology for manufacture the thermosyphon was based on Santos *et al.* (2014). The thermosyphon was produced by copper tube with an outer diameter of 12.7 mm, a wall thickness of 1 mm, and a total length of 500 (Figure 4). The lengths of evaporator and

the condenser are 150 and 350 mm, respectively. There is no adiabatic region. The thermosyphon was filled with 45.38 ml of deionized water.

Figure 4. Thermosyphon made of cooper.

Figure 5 shows the test rig which is composed by a copper thermosyphon, a power supply (Agilent™ U8002A), a data acquisition system (Agilent™ 34970A with 20 channels), a computer (Intel Core™ i5 3.30Ghz), an airflow fan (WMR™ P/N2123XST) and a digital anemometer (Minipa™ MDA-20).

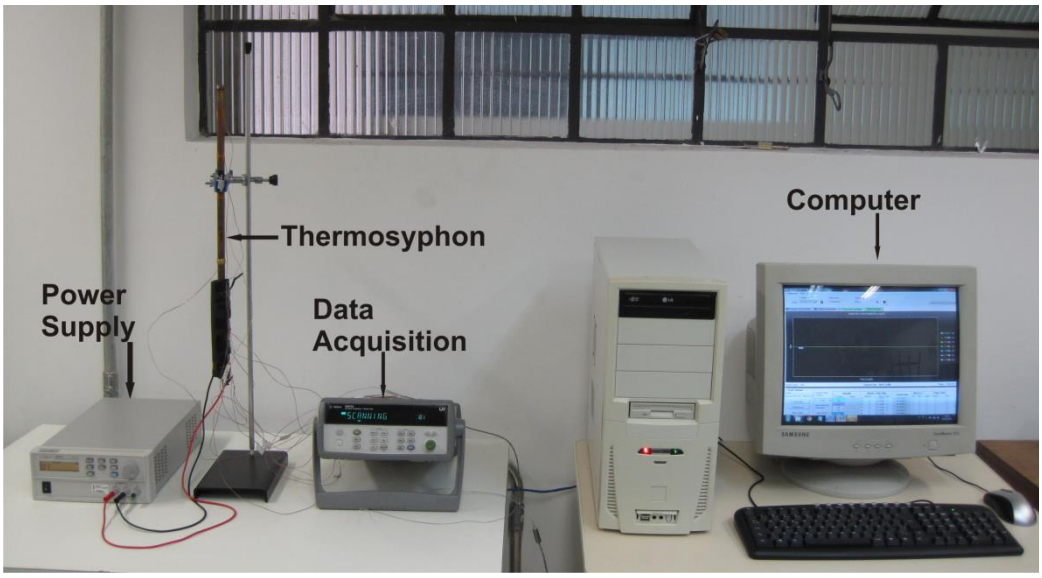

Figure 5. Test rig for the tests of copper thermosyphon cooled by air forced convection.

The evaporator of the thermosyphon was heated using a wire electric resistor (evaporator region at Figure 6) and the condenser was cooled by air forced convection. The heat load applied to the evaporator was varied from 30 to 60 W.

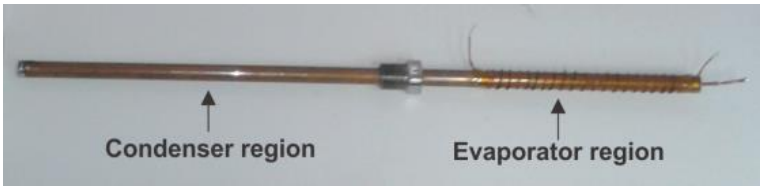

Figure 6. Condenser and evaporator regions.

The thermosyphon was tested at vertical position and a digital anemometer was used to measure the air velocity (approximately 5.6 m/s). The temperatures along the thermosyphon's outer surface were measured using 11 thermocouples (T-type): 4 thermocouples at the evaporator (T_{evap1}, T_{evap2}, T_{evap3}, and T_{evap4}), 4 thermocouples at the condenser (T_{cond1}, T_{cond2}, T_{cond3}, and T_{cond4}) and 3 thermocouples at the thermal insulation (T_{isol1}, T_{isol2}, and T_{isol3}), as shown in Figure 7.

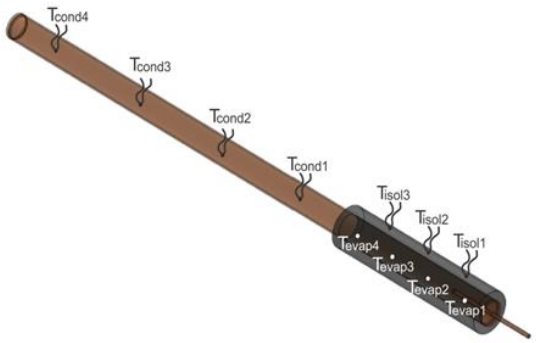

Figure 7. Thermocouples position on outer surface of thermosyphon and insulation.

The experimental uncertainties were estimated using the ISO-GUM method and taking into account the data acquisition and power supply uncertainties. Thus, the temperature uncertainty was estimated as ± 0.8 ºC and the uncertainty of the heat load applied to the evaporator was ± 0.53 W.

RESULTS

The experimental and theoretical results concerning the analysis of the thermosyphon are presented in this section.

Operation limits analysis

According to the mathematical model, for the operation temperature variation from 30 up to 110 ºC, the operation limits varied as shown in Figure 8. Figure 8(a) presents the entrainment, viscous, and sonic limits and in Figure 8 (b), the boiling limit is shown.

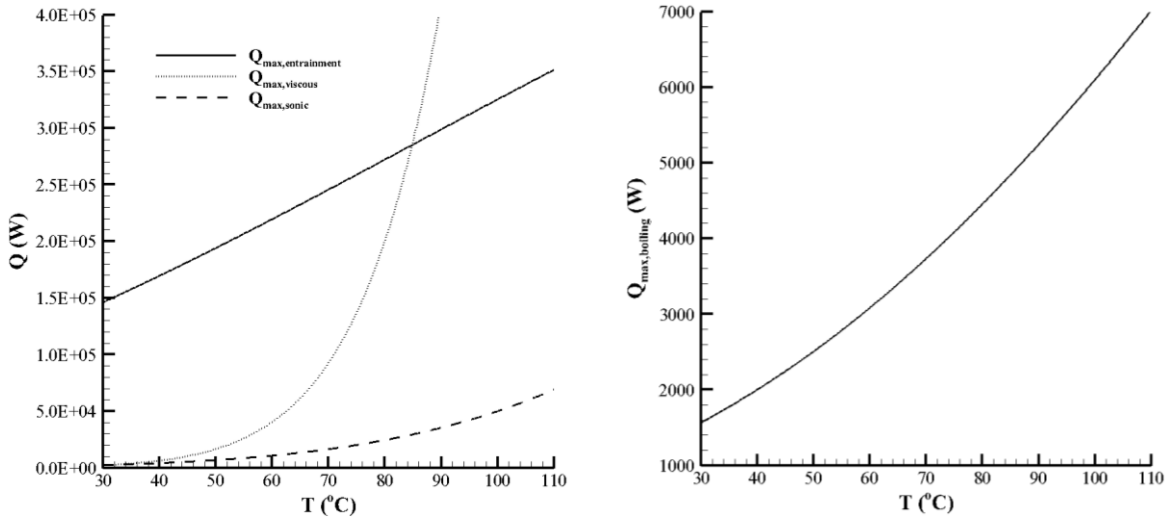

(a) (b)

Figure 8. Operation limits analsys: entrainment, viscous, and sonic limits (a) and boiling limit (b).

It is noticed that as the temperature increases all limits increase and the entrainment limit is the less restrictive limit until 85 ºC. After this temperature, 85 ºC, the viscous limit exceeds the entrainment limit, becoming the less restrictive limit. On the other hand, the ranges of sonic, viscous, and boiling limits are close together for the temperature variation from 30 to 45 ºC. In this temperature range, the boiling limit varied from 1,568 to 2,246 W; the viscous limit varied from 2,266 to 10,399 W; and the sonic limit varied from 2,486 to 5,404 W. Thus, as a result, the boiling limit was the most restrictive.

Temperature along the thermosyphon as a function of heat load

The experimental results as a function of the heat load applied in the evaporator region are presented in Figure 9.

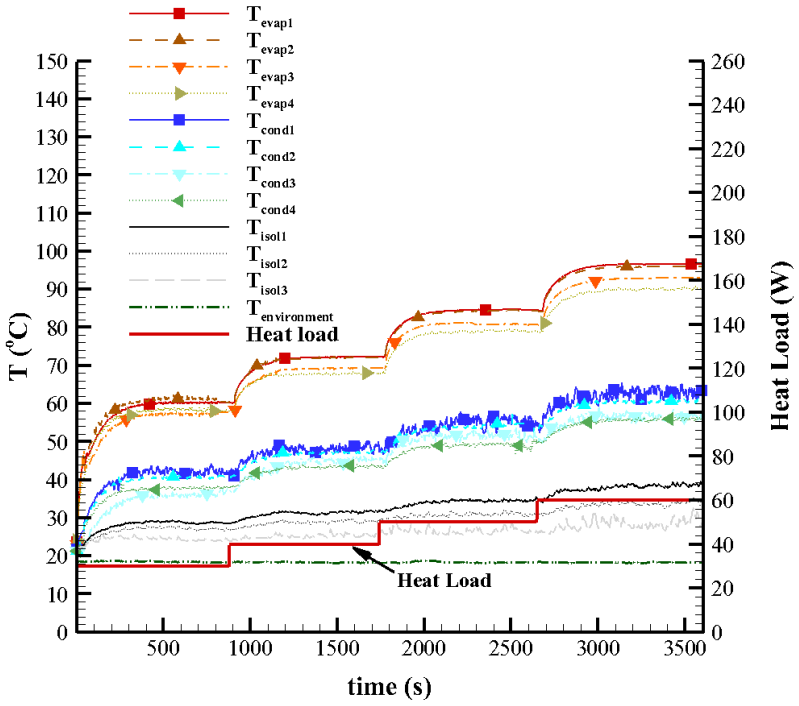

Figure 9. Temperature along the thermosiphon as a function of applied power and time

First, a heat load of 30 W was applied to the evaporator of the thermosyphon and it is noticed that all temperatures along the external surface of the thermosyphon (T_{evap1}, T_{evap2}, T_{evap3}, T_{evap4}, T_{cond1}, T_{cond2}, T_{cond3}, and T_{cond4}) increase fast. After approximately 100 s, the thermal behaviour of these temperatures trends to the steady state regime. Thus, it can be affirmed that it had a successful start-up. The steady state was reached at approximately 200 s.

After 15 min (900 s), the heat load was increased to 40 W and it is observed a similar thermal behaviour of the thermosyphon temperatures. The heat load was varied from 40 to 50 W and finally from 50 to 60 W. Note that for all heat loads applied, the thermosyphon

reached the steady state condition. The maximum temperature measured was 97 ºC in the evaporator region for heat load of 60 W. The maximum temperature measured in the condenser was 61 °C and in the insulation was 39 ºC both for 60 W.

Heat transfer analysis

Table 1 presents the results of the heat transfer analysis in function of the heat transfer rates: applied to the evaporator region, lost through the insulation and the thermosyphon wall, transferred into the thermosyphon and internal mass flow rate.

Table 1. Transfer heat rate.

$\dot{Q}_{evap}$ [W]	$\dot{Q}_{wall}$ [W]	$\dot{Q}_{isol}$ [W]	$\dot{Q}'_{evap}$ [W]	$\dot{m}_i \times 10^5$ [kg/s]
30	1.176	0.4246	28.40	1.20
40	1.440	0.5109	38.05	1.63
50	1.729	0.6892	47.58	2.06
60	2.034	0.8260	57.14	2.50

It is observed that when a heat load of 30 W was applied, 3.9 % of the heat was transferred through the tube wall, 1.4 % was transferred through the insulation, and 94.7 % was transferred into the evaporator of the thermosyphon. The estimated percentages for the other heat loads (40, 50, and 60 W) are very similar to these. Regarding on the internal mass flow rate, the variation is very small (order of 10^{-5} kg/s).

Analysis of the internal heat transfer coefficient in the condenser region

Table 2 presents the values of the internal heat transfer coefficients into the condenser region as a function of heat load.

Table 2. Internal heat transfer coefficients on the condenser area.

$\dot{Q}_{evap}$ [W]	$\bar{h}_{i,1}^{Cond} \times 10^{-4}$ [W/m²K]	$\bar{h}_{i,2}^{Cond} \times 10^{-4}$ [W/m²K]
30	1.52	3.09
40	1.46	3.29
50	1.43	3.44
60	1.41	3.56

From the two correlations presented before and the experimental data obtained through the heat transfer analysis, it is possible to estimate the coefficients in this section. $\bar{h}_{i,1}^{cond}$ is calculated using Eqs. (21), (23) and (24), and $\bar{h}_{i,2}^{cond}$ using Eqs. (25) to (27). Note that $\bar{h}_{i,1}^{cond}$ is 10 times greater than $\bar{h}_{i,2}^{cond}$. Thus, the value of $\bar{h}_{i,2}^{cond}$ is more conservative. However, it is necessary to develop a more sophisticated experiment in order to measure the inner heat transfer coefficient of the condenser region.

Comparison between theoretical and experimental results

In Figure 8, it is showed the theoretical results of the operation limits as a function of operation temperature variation (30 up to 110 ºC). Here, the real operation temperature was estimated, using Eq. (22), regarding the heat load applied to the evaporator.

Table 3 presents the maximum heat transfer rates for each operating limit taking into account the real operating temperature.

Table 3. Operation limits.

$\dot{Q}_{evap}$ [W]	T_{op} [°C]	$\dot{Q}_{max,entrainment}$ [W]	$\dot{Q}_{max,viscous}$ [W]	$\dot{Q}_{max,sonic}$ [W]	$\dot{Q}_{max,boiling}$ [W]
30	56.38	210,174	29,575	9,214	2,867
40	66.60	236,656	70,401	14,356	3,506
50	77.83	266,319	170,121	22,549	4,294
60	89.02	296,099	383,638	34,198	5,165

From Table 3, it is observed that the heat transfer rate obtained for the entrainment limit is the only limit that is much larger than the other limits for the applied heat load of 30 and 40 W. For 50 W and 60 W the scenario is quite different. For a heat load of 50 W, the viscous limit is only 1.5 times lower than the entrainment limit. Regarding the power of 60 W, the viscous limit becomes approximately 1.3 times greater than the entrainment limit. It is also observed that for all heat loads applied to the evaporator, the maximum heat transfer rates obtained for the boiling limit are the lowest one, varying from 2,867 to 5,165 W.

Therefore, it can be stated that the proposed thermosyphon could operate under higher heat loads than the ones applied. However, for security reasons it was not possible to accomplish these tests due to the temperature limitation imposed (maximum temperature of 120ºC).

CONCLUSIONS

This paper presented a theoretical and experimental analysis of a copper thermosyphon with deionized water as the working fluid. The device was cooled by air forced convection. Regarding the theoretical analysis, the entrainment, viscous, sonic, and boiling limits were evaluated for a temperature ranging from 30 to 110 ºC. It was observed in the analysis that the maximum heat transfer rates obtained were very high when compared to the heat load applied to the evaporator in the experiment. It was also noticed that the heat transfer rates obtained for the boiling limit were the less restrictive ones.

Regarding to the experimental analysis, the thermosyphon was tested at vertical position under heat loads of 30, 40, 50, and 60 W. The device worked satisfactorily obtaining successful start-up, and reaching steady state condition for all heat loads. The thermosyphon

took about 200 s to reach the steady state for heat load of 30 W and the maximum temperature of 97 ºC was measured at the evaporator region for 60 W.

A heat transfer analysis was performed using the experimental data obtained from the tests in which it was estimated the operating temperature inside the evaporator region (89 ºC for 60 W, for instance). The operating temperatures obtained in the experiments were used to determine the operating limits. For all the heat loads, the heat transfer rates were estimated for operating limits. The boiling limit was the lowest one, ranging from 2,867 to 5,165 W. Therefore, it can be affirmed that the thermosyphon developed here could operate under much higher heat loads without reaching any operating limit. However, for safety reasons it was not possible to perform such tests due to the experimental temperature limitation (120 ºC). The internal mass flow rate was estimated as an order of 10^{-5} kg/s.

Using specific correlations for thermosyphon condensers together with the mass flow rate calculated from the experimental results, it was possible to determine the internal heat transfer coefficient into the condenser region. The values estimated were in the order of 10^4 W/m^{2}K ($\bar{h}_{i,1}^{cond}$) and using the second method the values were in order of 10^3 W/m^{2}K ($\bar{h}_{i,2}^{cond}$).

Therefore, it can be concluded that the methodology of the development, test, and analyzing of the copper thermosyphon presented in this paper proved to be feasible.

REFERENCES

Abreu S. L. & Colle S. (2004). An experimental study of two-phase closed thermosyphons for compact solar domestic hot-water systems. *Solar Energy*, 76 (1), 141-145. doi:10.1016/j.solener.2003.02.001

Azad, E. (2008). Theoretical and experimental investigation of heat pipe solar collector. *Experimental Thermal and Fluid Science*, 32 (8), 1666–1672. doi:10.1016/j.expthermflusci.2008.05.011

Azad, E. (2012). Assessment of three types of heat pipe solar collectors. *Renewable and Sustainable Energy Reviews*, 16 (5), 2833-2838. doi:10.1016/j.rser.2012.02.001

Bergman, T.L., Lavine, A.S., Incropera, F.P. & DeWitt, D.P. (2012). *Fundamentals of heat and mass transfer.* New Jersey, USA: John Wiley & Sons.

Busse, C.A. (1973). Theory of the ultimate heat transfer limit on cylindrical heat pipes. *International Journal of Heat and Mass Transfer*, 16 (1), 169-186. doi:10.1016/0017-9310(73)90260-3

Chien C.C., Kung C.K., Chang C.C., Lee W.S., Jwo C.S. & Chen S.L. (2011). Theoretical and experimental investigations of a two-phase thermosyphon solar water heater. *Energy*, 36 (1), 415–423. doi:10.1016/j.energy.2010.10.023

Deng Y., Zhao Y., Wang W., Quan Z., Wang L. & Yu D. (2013). Experimental investigation of performance for the novel flat plate solar collector with micro-channel heat pipe array (MHPA-FPC). *Applied Thermal Engineering*, 54 (2), 440-449. doi:10.1016/j.applthermaleng.2013.02.001

Du, B., Hu, E. & Kolhe, M. (2013). An experimental platform for heat pipe solar collector testing. *Renewable and Sustainable Energy Reviews*, 17, 119-125. doi:10.1016/j.rser.2012.09.009

Groll, M. & Rosler, S. (1992). Operation principles and performance of heat pipes and closed two-phase thermosyphons. ***Journal of Non-Equilibrium Thermodynamics***, 17 (2), 91-151. doi:10.1515/jnet.1992.17.2.91

Hussein H. M. S., Mohamad M. A. & El-Asfouri A. S. (1999a). Optimization of a wickless heat pipe flat solar collector. *Energy Conversion and Management*, 40 (18), 1949-1961. doi:10.1016/S0196-8904(99)00082-5

Hussein H. M. S., Mohamad M. A. & El-Asfouri A. S. (1999b). Transient investigation of a thermosyphon at-plate solar collector. *Applied Thermal Engineering*, 19 (7), 789-800. doi:10.1016/S1359-4311(98)00085-4

Ismail K. A. R. & Abogderah M. M. (1998). Performance of a heat pipe solar collector. *Journal of Solar Energy Engineering*, 120 (1), 51-59. doi:10.1115/1.2888047

Mantelli, M. H. B. (2013). *Thermosyphon technology for industrial applications.* In: Vasiliev L. L. & Kakaç, S. (Eds.). *Heat pipes and solid sorption transformations: fundamentals and practical applications*. Chapter 11. New York, USA: CRC Press.

Oliveti G. & Arcuri N. (1996). Solar radiation utilisability method in heat pipe panels. *Solar Energy*, 57 (5), 345-360. doi:10.1016/S0038-092X(96)00109-0

Peteson, G.P. (1994). *Heat pipes: modeling, testing, and applications.* Toronto, CAN: John Wiley & Sons.

Santos, P.H.D., Krambeck, L., Santos, D.L.F. & Antonini Alves, T. (2014). Analysis of a stainless steel heat pipe based on operation limits. *International Review of Mechanical Engineering*, 8 (3), 599-608. doi: http://dx.doi.org/10.15866/ireme.v8i3.902